Anatomically and mechanically accurate scala tympani model for electrode insertion studies

Anastasiya Starovoyt , Eman Shaheen , Tristan Putzeys , Greet Kerckhofs , Constantinus Politis , Jan Wouters , Nicolas Verhaert

PII: S0378-5955(23)00019-9
DOI: https://doi.org/10.1016/j.heares.2023.108707
Reference: HEARES 108707

To appear in: *Hearing Research*

Received date: 27 July 2022
Revised date: 25 November 2022
Accepted date: 24 January 2023

Please cite this article as: Anastasiya Starovoyt , Eman Shaheen , Tristan Putzeys , Greet Kerckhofs , Constantinus Politis , Jan Wouters , Nicolas Verhaert , Anatomically and mechanically accurate scala tympani model for electrode insertion studies, *Hearing Research* (2023), doi: https://doi.org/10.1016/j.heares.2023.108707

Anatomically and mechanically accurate scala tympani model for electrode insertion studies

Anastasiya Starovoyt [a, b] (anastasiya.starovoyt@gmail.com),
Eman Shaheen [c, d] (eman.shaheen@uzleuven.be),
Tristan Putzeys [a, b, e] (tristan.putzeys@kuleuven.be),
Greet Kerckhofs [f, g, h, i] (greet.kerckhofs@uclouvain.be),
Constantinus Politis [c, d] (constantinus.politis@kuleuven.be),
Jan Wouters [a, b] (jan.wouters@kuleuven.be),
Nicolas Verhaert [a, b, j, 1] (nicolas.verhaert@kuleuven.be)

Author affiliations:

a. Research Group Experimental Oto-Rhino-Laryngology, Department of Neurosciences, KU Leuven, University of Leuven, Leuven, Belgium
b. Leuven Brain Institute, Department of Neurosciences, KU Leuven, 3000 Leuven, Belgium
c. OMFS IMPATH Research Group, Department of Imaging and Pathology, KU Leuven, University of Leuven, Leuven, Belgium
d. Department of Oral and Maxillofacial Surgery, UZ Leuven, University Hospitals Leuven, Leuven, Belgium
e. Laboratory for Soft Matter and Biophysics, Department of Physics and Astronomy, KU Leuven, University of Leuven, Leuven, Belgium
f. Biomechanics lab, Institute of Mechanics, Materials, and Civil Engineering, UCLouvain, Louvain-la-Neuve, Belgium
g. Department of Materials Engineering, KU Leuven, University of Leuven, Leuven, Belgium
h. IREC, Institute of Experimental and Clinical Research, UCLouvain, Woluwé-Saint-Lambert, Belgium
i. Prometheus, Division of Skeletal Tissue Engineering, KU Leuven, University of Leuven, Leuven, Belgium
j. Department of Otorhinolaryngology, Head and Neck Surgery, UZ Leuven, University Hospitals of Leuven, Leuven, Belgium

[1)]Corresponding author:

Nicolas Verhaert
ExpORL, Dept. Neuroscience, KU Leuven
Onderwijs en Navorsing 2 (O&N2)
Herestraat 49 bus 721
B-3000 Leuven
Belgium
Tel.: +32 16 37 78 53
email: nicolas.verhaert@kuleuven.be

Highlights

- Electrode insertion trauma compromises CI performance and residual hearing
- Risk of trauma depends on individual cochlear anatomy and insertion mechanics
- Understanding of electrode insertion mechanics is crucial to prevent trauma
- Cochlear models enable controlled, repeatable electrode insertion studies
- Insertion forces and tactile feedback are complementary for mechanical evaluation
- Individual anatomy affects insertion peak force, end resistance and insertion depth

Abstract

The risk of insertion trauma in cochlear implantation is determined by the interplay between individual cochlear anatomy and electrode insertion mechanics. Whereas patient anatomy cannot be changed, new surgical techniques, devices for cochlear monitoring, drugs, and electrode array designs are continuously being developed and tested, to optimize the insertion mechanics and prevent trauma. Preclinical testing of these developments is a crucial step in feasibility testing and optimization for clinical application. Human cadaveric specimens allow for the best simulation of an intraoperative setting. However, their availability is limited and it is not possible to conduct repeated, controlled experiments on the same sample. A variety of artificial cochlear models have been developed for electrode insertion studies, but none of them were both anatomically and mechanically representative for surgical insertion into an individual cochlea. In this study, we developed anatomically representative models of the scala tympani for surgical insertion through the round window, based on microCT images of individual human cochleae. The models were produced in transparent material using commonly-available 3D printing technology at a desired scale. The anatomical and mechanical accuracy of the produced models was validated by comparison with human cadaveric cochleae. Mechanical evaluation was performed by recording insertion forces, counting the number of inserted electrodes and grading tactile feedback during manual insertion of a straight electrode by experienced cochlear implant surgeons. Our results demonstrated that the developed models were highly representative for the anatomy of the original cochleae and for the insertion mechanics in human cadaveric cochleae. The individual anatomy of the produced models had a significant impact on the insertion mechanics. The described models have a promising potential to accelerate preclinical development and testing of atraumatic insertion techniques, reducing the need for human cadaveric material. In addition, realistic models of the cochlea can be used for surgical training and preoperative planning of patient-tailored cochlear implantation surgery.

Keywords

cochlear implantation; electrode insertion trauma; scala tympani model; round window approach; 3D printing; microCT imaging

1. Introduction

Cochlear implants (CI) are an established treatment for patients with severe to profound hearing loss. These neuro-implants enable impressive restoration of speech understanding in subjects with both partial and complete hearing loss by directly stimulating the auditory nerve from within the cochlea (Lenarz, 2017). However, when the stimulating electrode of the CI is inserted into the cochlea, it can easily traumatize intracochlear structures. Electrode insertion trauma occurs in up to 32% of insertions (Hoskison et al., 2017), negatively affecting the CI performance and compromising residual hearing function in patients with partial hearing loss (Bas et al., 2012). Individual cochlear anatomy has a large impact on the mechanics of insertion and the risk of trauma (Avci et al., 2014; Demarcy et al., 2017; Verbist et al., 2009). Whereas patient anatomy cannot be changed, new surgical techniques, devices for cochlear monitoring, drugs, and electrode array designs are continuously being developed and tested, to optimize the insertion mechanics and avoid trauma (De Seta et al., 2022).

Preclinical testing is usually done on human cadaveric cochleae (Briggs et al., 2011; Snels et al., 2021). Cadaveric cochleae are considered the best model of the living cochlea, since they are highly representative for the anatomical variability and insertion mechanics in real patients. However, post mortem changes of the intracochlear structures, such as oedema and necrosis of the epithelium, can alter physical properties of the tissues and thus the mechanics of electrode insertion. Cadaveric specimens also cannot be used for repeated electrode insertions, because insertion trauma can immediately affect the insertion trajectory and mechanics of subsequent experiments, yielding unreliable results. Furthermore, the position of the electrode array cannot be directly visualized and controlled inside the human cochlea due to bone encapsulation, unless the cochlea is either surgically opened, optically cleared (Tinne et al., 2017), imaged or processed for histological analysis (Briggs et al., 2011). In addition, cadaveric cochleae cannot be scaled up to test the feasibility of new prototypes, which have not yet been miniaturized (Zhang et al., 2010). The availability of human cadaveric specimens is also very limited and highly regulated (Roosli et al., 2013).

To tackle these limitations and to enable controlled, repeatable electrode insertions in preclinical studies, a variety of cochlear models have been developed. These models are based on the anatomy of the spiral-shaped scala tympani (ST) compartment of the cochlea, into which the electrode array is typically inserted during CI surgery (Lenarz, 2017), and can be grossly divided into two groups: geometrical models and anatomical models. Geometrical models mimic the anatomy of the human cochlear spiral with geometrical shapes (Clark et al., 2011; Leon et al., 2014; Majdani et al., 2010b; Todd et al., 2007; Zhang et al., 2010). Leon et al. developed scalable 3D printed geometrical models based on average reported dimensions of the ST (Clark et al., 2011; Leon et al., 2014). In addition, the authors designed two versions of their model, corresponding to the two possible surgical approaches for electrode insertion. The round window (RW) version simulates the insertion through the round window membrane (the only part of the cochlea, which is not covered by bone); the cochleostomy version simulates insertion through a surgically drilled tunnel, just below the RW. Yet, any mathematical design, even when based on real anatomical data, reduces the complexity of the real 3D shape of the ST. Furthermore, one model by design cannot represent the inter-individual anatomical variability, which is a very important factor for the insertion mechanics and trauma (van der Marel et al., 2014). Contrary to the geometrical models, anatomical models attempt to accurately replicate the anatomy of real individual cochleae (Aebischer et al., 2021; Rebscher et al., 1996). Rebscher et al., developed anatomical ST models by making casts of real human cadaveric cochleae (Rebscher et al., 1996). However, the authors reported that due to limitations of the casting

technique these models could not be scaled up by more than 14%, whereas it can desirable to achieve at least a scale of 3:1 for development and testing of new prototypes (Zhang et al., 2010). Furthermore, the surgical access for electrode insertion was not incorporated into the model design. Aebischer et al. recently reported on fabrication of scalable, anatomical ST models, based on computed tomography (CT) and microfocus CT (microCT) data, using a combination of 3D printing and casting technology (Aebischer et al., 2021). These models were tested with custom-made electrode array dummies and the authors suggested mounting separate artificial parts onto the model to simulate different surgical approaches. However, the modelling of the surgical approach was not tested and demonstrated in the study, and it is unclear whether these models can also be used with existing clinical electrode arrays. In addition to the shape of the ST, it is important to accurately model the intracochlear fluid within it. This fluid also plays an important role for the friction forces during electrode insertion into a real human cochlea (Kontorinis, Paasche, et al., 2011; Rebscher et al., 1996; Todd et al., 2007). Different solutions have been proposed in the past to achieve more representative friction forces in cochlear models, such as saline solution (Kontorinis, Lenarz, et al., 2011; Kontorinis, Paasche, et al., 2011; Leon et al., 2014), soap solution (Aebischer et al., 2021; Kontorinis, Paasche, et al., 2011; Majdani et al., 2010a; Rebscher et al., 1996; Todd et al., 2007) and glycerine (Kontorinis, Paasche, et al., 2011; Zhang et al., 2010).

The objective of this study was to develop physical models, which are anatomically, surgically and mechanically representative for electrode insertion into a real human cochlea. In addition, the developed models had to be scalable, transparent and robust, to enable repeated, controlled testing of existing electrode arrays and next-generation prototypes. In light of the latest evidence, we primarily focused on the RW surgical approach, since it is considered the least traumatic and therefore the most favorable for CI patients (Roland et al., 2007; Schart-Morén et al., 2019). We hypothesized that a representative model of RW insertion can be developed by replicating the anatomy of the ST and the RW in an individual cochlea. This was achieved by designing the models based on microCT images of human cadaveric cochleae. To validate the 3D printed models, their anatomy at the scale 1:1 was compared to the original microCT data and the insertion mechanics were compared to six human cadaveric cochleae and the RW models of (Leon et al., 2014), further referred to as the *'Leon models'*.

2. Methods

2.2. Samples

To evaluate whether 3D printing technology can capture the interindividual differences in cochlear anatomy, we developed models based on samples originating from two individuals. One temporal bone specimen (TB1) was obtained from an anonymous donor at the Vesalius Institute of the University of Leuven, and another (TB2) was retrieved from a clinical brain autopsy subject at the University Hospitals of Leuven. The harvesting and the use of the TBs was conducted in accordance with the Helsinki declaration and approved by the Medical Ethics Committee of the University Hospitals of Leuven (approval No. NH019 2016-06-04). TB1 was a right-sided, fixed specimen, wherein the RW membrane was accessed through surgical mastoidectomy, enlarged posterior tympanotomy and removal of the bony overhang. TB2 was a left-sided, fresh-frozen specimen, wherein the inner ear was isolated after the surgical mastoidectomy (Starovoyt et al., 2019).

2.3. MicroCT imaging and processing

High-resolution microCT images of TB1 and TB2 were acquired over 360° using a Phoenix NanoTom S (GE Measurement and Control Solutions, Germany) with a diamond-coated tungsten target (Appendix 1 Fig. A1). To visualize intracochlear soft tissues, in TB1, the intracochlear fluid was aspirated through a small opening in the RW membrane; in TB2, the isolated inner ear was submersed in Hafnium-substituted Wells-Dawson polyoxometalate ($K_{16}[Hf(\alpha_2\text{-}P_2W_{17}O_{61})_2]\cdot 19H_2O$) in phosphate-buffered saline solution for 3 days (Kerckhofs et al., 2018). The 3D printed models were also imaged in a similar way to evaluate the printing accuracy. The details of the microCT acquisition parameters are provided in Table 1.

	filter	voltage (keV)	current (µA)	isotropic voxel size (µm)	number of images	frame averaging	scan type	source-detector distance (mm)	exposure time (ms)	scanning time (hh:mm)
TB1	Al 0.5mm	100	410	9.8	2400	1	fast	600	500	00:20
TB2	-	50	531	6.3	2400	3	long	266	500	01:26
models	-	40	664	6.3	2400	1	fast	266	500	00:20

Table 1. MicroCT acquisition parameters.

The microCT data were reconstructed in Datos|x (GE Sensing & Inspection Technologies GmbH, Wunstorf, Germany), while applying scan optimization (projection filter, inline volume filter, and beam hardening correction). The files were exported as 16-bit .tiff slices and converted to .jpeg images, whereby histogram window was automatically adjusted to the dynamic range of the dataset using an in-house developed MatLab tool (MathWorks, MA, USA) (Maes et al., 2022). The data were cropped to the cochlear region in CTAn (Bruker MicroCT, Kontich, Belgium) and reoriented in accordance with the cochlear coordinate system (Verbist et al., 2010) in DataViewer (Bruker MicroCT, Kontich, Belgium), whereby the rotation axis goes through the center of the cochlear modiolus and the 0° angle is set at the center of the RW. After that, the datasets of TB1 and TB2 were resized to an isotropic voxel size of 19.6 µm and 18.9 µm respectively in CTAn.

2.4. Development of the ST models

The models were designed based on segmentation of the ST and the RW membrane from microCT images of human temporal bones TB1 and TB2. Therefore, we refer to these models as the '*microCT models*'.

MIMICS software (version 22.0, Materialise, Leuven, Belgium) was used to manually segment the ST and the RW membrane from microCT datasets of TB1 and TB2, using built-in interpolation algorithm (Appendix 1 Fig. A2). In TB1, the ST could not be segmented beyond the first two cochlear turns, because the thin soft tissues, separating the ST from the SV could not be sufficiently visualized; in TB2, the ST was segmented throughout the entire cochlea. After the segmentation, the datasets of the ST and the RW membrane were saved as two separate .stl files.

We assessed the general anatomical characteristics of the two samples against the population of the human cochleae: the width, length, height of the cochlear spiral, the total cochlear volume and the number of cochlear turns. The width, length and height were measured manually in DataViewer, the number of cochlear turns was measured manually on segmented data in 3-matic software (version 18.0, Materialise, Leuven, Belgium), and the total cochlear volume was calculated automatically based on a fast thresholding-segmentation of the entire cochlea in MIMICS software. Each manual measurement was carried out three times, and the averaged values were compared against the cochlear dimensions reported in the literature.

The ST models were developed in 3-matic software by modelling a semi-uniform wrapping around the hollow ST segment with two openings: a proximal opening in the shape and position of the RWM

and a distal circular opening at the apical end of the ST with a diameter of 1 mm. Two wrapping thicknesses were investigated: 0.5 mm and 0.3 mm (at the scale 1:1). In the 0.3 mm models, the proximal ST segment was additionally stabilized, by connecting its outer wall to the rest of the model. In the 0.5 mm models, the wrapping thickness around the RW was adjusted to 0.3 mm, to enable electrode insertion through the RW without additional surgical drilling. The developed models were saved as .stl files for printing.

2.5. 3D printing of the ST models

The models were 3D-printed with two different types of additive manufacturing methods: material jetting (MJ) with internal and external support material and stereolithography (SLA) with only external support structure. To facilitate subsequent surgical-mechanical evaluation, we mirrored the model of the TB2 to have two right-sided models. Photographs of the printed 3D models are provided in Fig. 1.

Figure 1. Photograph of the 3D printed SLA and MJ models with the wrapping thickness 0.3 mm and 0.5 mm of the TB1 and TB2. The stabilizing segment in the 0.3 mm models is indicated with a red arrow. (scale bar: 5 mm)

The MJ models were printed with transparent VeroClear (RGD810) material with Sup705 support material, using the Objet Connex 350 3D Printer (Stratasys, Eden Prairie, MN, USA) with a minimum layer thickness of 16µm. The external support material was mechanically rinsed from the models. To remove the internal support material from the ST lumen of the MJ models, they were submersed in a 40% sodium hydroxide (NaOH) solution for two days, whereby they were placed on an ultrasonic cleaner and flushed with a syringe several times a day.

The SLA models were printed with Anycubic translucent UV resin, using the Anycubic Photon S 3D printer (Anycubic Technology Co., Ltd., Shenzhen, China) with a minimum layer thickness of 25µm. Prior to printing, the external support structure at the base of the cochlea was added using the Photon Slicer software. After printing, the models were washed with isopropanol 99,8% solution and hardened in a UV-curing box (10W, 390-410 nm) for 2 hours. The external support material structure was carefully cut from the printed models with a side cutter.

2.6. Anatomical evaluation of the ST models

The anatomical accuracy of the developed microCT models was evaluated before (segmentation accuracy) and after 3D printing (printing accuracy), as illustrated in Fig. 2, and expressed as a root mean square error (RMSE).

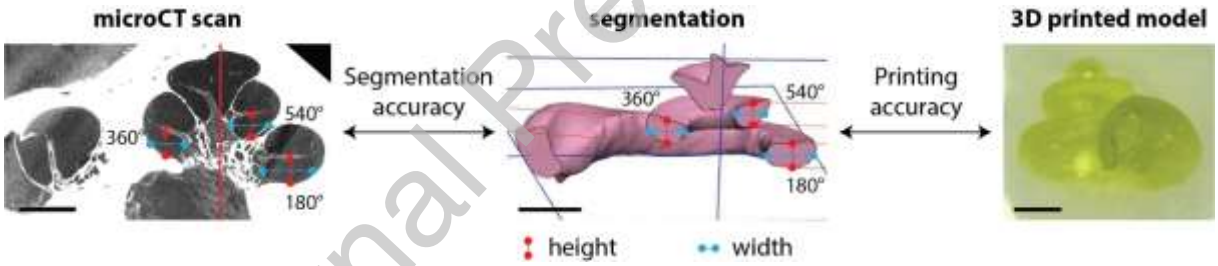

Figure 2. Evaluation of the anatomical accuracy in TB2. The anatomical accuracy was evaluated by comparing the microCT scan of the original cochlea with its segmentation (segmentation accuracy), and the morphology of the 3D printed model with the segmentation of the original cochlea (printing accuracy). To determine the accuracy of the ST dimensions, the central height and width of the ST were measured at 180°, 360° and 540° on the microCT slices and the segmentation, as well as on the microCT slices of the 3D printed model. To compare the global shape of the 3D printed model with the original cochlea, the segmentation of the printed model was compared to the segmentation of the original cochlea (printing accuracy). (scale bars: 2 mm)

The segmentation accuracy was assessed by comparing the dimensions of the segmented ST to the original microCT data of the cochleae from temporal bones TB1 and TB2. The central height and width of the ST was measured manually (in Dataviewer for the microCT data; in 3-matic software for the segmented ST) at 180°, 360° and 540° from the center of the RW membrane in accordance with the cochlear coordinate system (Verbist et al., 2010). Each measurement was carried out three times. Comparison of the ST dimensions on the microCT slices of the models to the segmentation of the original cochlea was performed using Wilcoxon signed rank test. The difference was considered significant if the resulting p-value was ≤ 0.05.

To evaluate printing accuracy, 3D printed models with different characteristics (TB1 and TB2 anatomy, 0.3 mm and 0.5 mm wrapping thickness, SLA and MJ printing method) were imaged with microCT and compared to the original cochleae. On the one hand, the ST dimensions of the printed models were evaluated against the original segmented cochleae analogous to the evaluation of the segmentation accuracy. On the other hand, we assessed the differences in the global ST shape between the models and the cochleae using singed part comparison analysis in 3-matic software. The segmented ST of the model was manually aligned with the ST segment of the original cochlea by an experienced operator, and the overall distance between the surfaces was evaluated using a color-coded map and represented by a single measurement, the root mean square error (RMSE).

2.7. Mechanical evaluation of the ST models

The mechanical accuracy of the models was assessed in electrode insertion experiments, using a soft straight 23 mm HiFocus™ SlimJ electrode array (Advanced Bionics LLC, Valencia, USA) with an inter-electrode distance of 1.3 mm (Advanced Bionics, n.d.). MicroCT models with different characteristics were compared to the Leon model and to six human cadaveric cochleae. All insertions (N = 108) were performed manually through the RW by four operators: one researcher, trained in CI surgery (operator 1) and three experienced CI surgeons (operators 2-4). Each operator received his/her own electrode, which was inspected and straightened, if necessary, after each insertion. The same ST models were used by all operators in all experiments.

The following model characteristics were evaluated: (1) the fluid: physiological saline solution (0.9% NaCl) versus 10% soap solution; (2) the printing method: SLA versus MJ; (3) model design: microCT versus Leon; (4) wrapping thickness (for microCT models only): 0.3 mm versus 0.5 mm; (5) model anatomy (for microCT models only): TB1 versus TB2. For each insertion, we recorded a video of the insertion, the number of non-inserted electrodes, the insertion forces and the surgical tactile feedback. The insertion mechanics were evaluated based on the following parameters: peak forces during the insertion, the number of inserted electrodes and the surgical tactile feedback.

The insertion forces were measured at the level of the models and the cochleae, which were fixated with dental wax onto a piezoresistive force sensor (166H-1kg BCM Sensor technologies BVBA, resolution 0.05 mN), similar to previously described setups (Aebischer et al., 2022; Majdani et al., 2010a). The exerted forces on the sample caused by the insertion of the electrode were automatically recorded every 0.1 s, using an in-house developed Matlab tool.

The surgical tactile feedback was graded by comparing the experienced resistance during each insertion to either real-life CI surgery (the surgeons) or fresh-frozen cochleae (the researcher). The tactile feedback in human cadaveric cochleae, in comparison to real-life CI surgery, was only assessed by the CI surgeons, and not by the researcher. The resistance was evaluated at the following points: (1) at the RW, (2) at the first cochlear turn, (3) at the end of the insertion and (4) throughout the entire insertion. The following 7-point scale was applied, to compare the experienced resistance to real-life CI surgery (or fresh-frozen cochleae): 0 = identical to CI surgery; ± 1, slightly higher/lower; ± 2, substantially higher/lower; ± 3 much higher/lower than CI-surgery.

The mechanical accuracy of the models was evaluated in R software. Firstly, we determined which model characteristics had an effect on the mechanical outcome parameters. Linear mixed model analysis was performed for each outcome parameter in a step-wise fashion (Appendix 2) to determine which model characteristics had an impact on the insertion mechanics and which

combination of model characteristics was the most representative for a real cochlea. The operator performing the insertion was set as a fixed effect. After that, we compared the microCT and the Leon models with the best model characteristics – SLA method and soap solution – to the cadaveric cochleae by using non-paired t-test with unequal variances. Finally, we investigated whether the different anatomy and wrapping thickness had an effect on the insertion mechanics in microCT models, by performing linear mixed model analysis (Appendix 2, step 4). Sensitivity analysis was performed using equivalent non-parametric tests (robust linear mixed model analysis and Wilcoxon signed rank test) and led to the same outcomes in terms of significance. P-values were considered significant if ≤ 0.008333, after applying Bonferroni correction for multiple testing of the six mechanical outcome parameters.

2.9. Figures

All graphical representations were made in Graphpad Prism. The final figures were created in Adobe Illustrator.

3. Results

3.1 Anatomical characteristics of the human cochlea samples

The results of the anatomical evaluation are summarized in Table 2. TB2 was larger than TB1 and had also a larger number of cochlear turns. The dimensions of both cochleae were well within the ranges, which were previously reported in the literature.

	TB1	**TB2**	**range in the literature**
length (mm)	8.3	9.5	8.0 – 10.1 (Avci et al., 2014; Dhanasingh et al., 2021; Shin et al., 2013)
width (mm)	6.4	6.8	5.6 – 8.2 (Avci et al., 2014; Dhanasingh et al., 2021; Erixon et al., 2009; Shin et al., 2013)
height (mm)	4.2	4.2	3.3 – 4.8 (Avci et al., 2014; Erixon et al., 2009; Shin et al., 2013)
volume (mm^3)	75.2	81.3	50.8 – 118.5 (Conde-Valverde et al., 2019; Kendi et al., 2005; Kirk & Gosselin-Ildari, 2009; Takahashi et al., 2018)
number of turns	2.4	2.8	2.2 – 2.9 (Avci et al., 2014; Conde-Valverde et al., 2019; Erixon et al., 2009; Shin et al., 2013)

Table 2. Anatomical characteristics of the human cochlea samples.

3.2. Anatomical accuracy of the ST models

3.2.1. Segmentation accuracy

The ST dimensions did not significantly differ between the original microCT data and the segmentation of the ST ($p \geq 0.06$). According to the results summarized in Appendix 1 Table A1 and visualized in Fig. 2, the correspondence between the segmentation and the original microCT data was better in TB2, which was segmented from contrast-enhanced microCT images, due to a better soft tissue visualization, which was achieved with contrast-enhanced microCT (Appendix 1 Fig. A1).

3.2.2. Printing accuracy

MicroCT imaging study of the models (Appendix 1 Fig. A3) revealed that the SLA models were characterized by a smooth surface, whereas the MJ models expressed 'hairy' irregularities, resulting from mechano-chemical removal of the internal support material.

Comparative analysis of the ST dimensions showed that the MJ models generally corresponded well to the original cochleae, despite the erosion (Fig. 3). In the SLA models, the ST compartment was undersized to a variable extent compared to the ST segmentation of the corresponding cochlea.

The results of part comparison analysis between the internal ST surface of the 3D printed models and the corresponding cochleae are depicted in Fig. 4. Color-coded maps confirmed that the SLA models were overall undersized (majority of deviation below 0 mm), whereas in the MJ models the majority of surface points aligned well with the original cochleae (median deviation around 0 mm). RMSE varied between 0.05 mm – 0.13 mm, and was comparable for the SLA and the MJ models. Larger individual deviations between the closest points of the two surfaces (max. 0.36 mm) were seen in the proximal ST region of the models, whereby the orientation of the entire region was slightly shifted due to a warping deformation during printing.

3.3. Mechanical accuracy of the ST models

Snapshots of electrode insertion experiments in different samples with their respective insertion force profiles are illustrated in Fig. 5A-B.

3.3.1. The best model characteristics

Our results showed that the fluid and the printing method had a statistically significant effect on the insertion mechanics ($p < 0.008$ for least one of the mechanical parameters), irrespective of the model design, anatomy and wrapping thickness (Appendix 2). When the models were filled with saline solution, on average only 8.9 out of 16 electrodes could be inserted and all operators reported a very high end resistance (grade 3). In the models with soap, on average 14.8 electrodes could be inserted and the end resistance was graded on average 1.5. However, this tactile feedback did not correspond to the measured peak insertion forces, which were much higher for the (deeper) insertions in models with soap (mean = 77.3 mN), compared to the models with saline solution (mean = 24.5 mN). The SLA models with soap showed the best correspondence to the real human cochleae and were therefore used for further comparison. The surgeons reported that contrary to the SLA models, the insertion into the MJ models was less smooth and characterized by jittering movement, even when full insertion could nevertheless be achieved.

3.3.2. MicroCT models versus Leon models

Comparison of the microCT and the Leon models to the human cadaveric cochleae showed that they were not significantly different from the real cochleae for any of the mechanical parameters (Fig. 5C). In the Leon models, the surgically perceived end resistance (mean = 0.5) was substantially lower than in the real human cadaveric cochleae (mean = 1.5) and the microCT models (mean = 1.7), but closer to the living cochlea (value 0 according to our scale). However, after applying Bonferroni correction, this difference was considered not significant.

3.3.3. The effect of anatomy on insertion mechanics

Finally, we evaluated whether different anatomy and wrapping thickness had an effect on the insertion mechanics in the microCT models. As expected, the wrapping thickness had no significant effect on the insertion mechanics (Appendix 2). There was however a significant difference in the number of inserted electrodes and the experienced resistance at the end of the insertion between the models TB1 and TB2 (Fig. 5D). On average 1.4 more electrodes could be inserted into TB1, which corresponds to a 1.82 mm deeper insertion, and also resulted in on average 25.6 mN higher insertion forces. This mechanical difference could be explained by the overall size of the cochlea (TB2 is larger

according to Table 2), but rather by the individual anatomy of the ST compartment (narrower height and width according to Fig. 3).

A Measured ST dimensions in the original cochleae and the 3D printed models

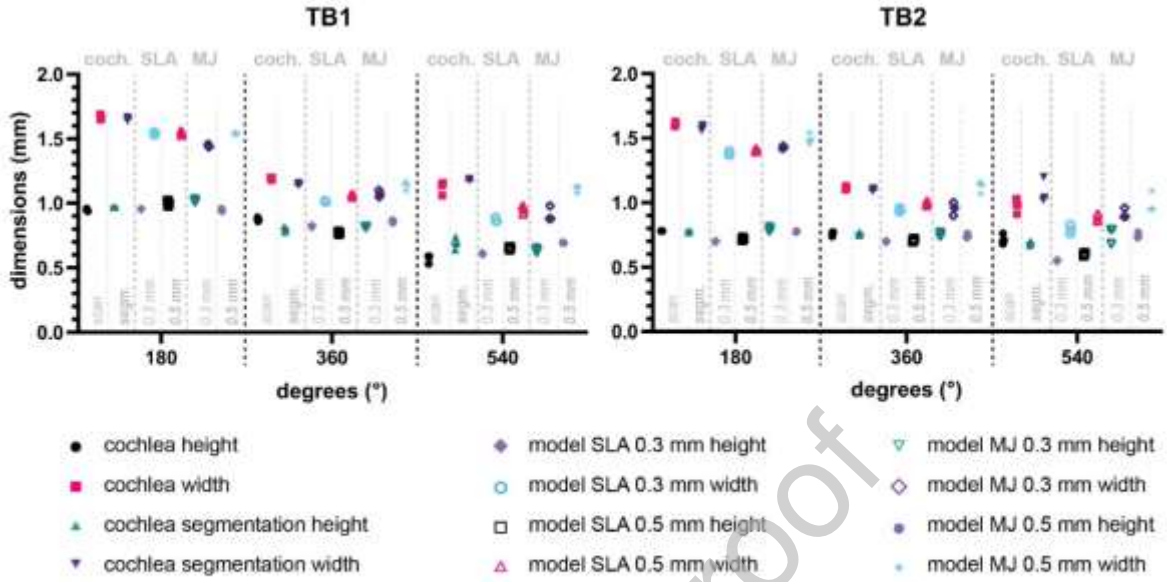

B Comparison of 3D printed models to the original cochleae

TB1	cadaveric cochleae (N = 3)		SLA models (N = 6)			MJ models (N = 6)		
	mean	range	mean	range	p-value	mean	range	p-value
180° height (mm)	0.97	0.97-0.97	0.98	0.95-1.02	1.00	0.98	0.94-1.03	1.00
180° width (mm)	1.66	1.64-1.67	1.54	1.53-1.56	0.03*	1.49	1.44-1.55	0.03*
360° height (mm)	0.80	0.78-0.82	0.80	0.76-0.83	1.00	0.84	0.81-0.87	0.15
360° width (mm)	1.15	1.14-1.16	1.04	1.01-1.07	0.03*	1.11	1.05-1.14	0.36
540° height (mm)	0.69	0.64-0.74	0.63	0.60-0.66	0.09	0.66	0.62-0.70	0.52
540° width (mm)	1.18	1.18-1.19	0.91	0.86-0.98	0.03*	1.01	0.88-1.13	0.03*

TB2	cadaveric cochleae (N = 3)		SLA models (N = 6)			MJ models (N = 6)		
	mean	range	mean	range	p-value	mean	range	p-value
180° height (mm)	0.78	0.77-0.78	0.71	0.69-0.73	0.03*	0.78	0.77-0.81	0.51
180° width (mm)	1.58	1.56-1.60	1.40	1.37-1.42	0.03*	1.46	1.42-1.54	0.03*
360° height (mm)	0.76	0.75-0.77	0.71	0.69-0.72	0.03*	0.75	0.73-0.77	0.24
360° width (mm)	1.10	1.09-1.11	0.97	0.93-1.01	0.03*	1.04	0.90-1.16	0.51
540° height (mm)	0.69	0.67-0.70	0.58	0.54-0.61	0.03*	0.75	0.68-0.79	0.09
540° width (mm)	1.09	1.02-1.20	0.83	0.76-0.91	0.03*	0.96	0.89-1.09	0.09

* Significant $p \leq 0.05$

Figure 3. Assessment of the segmentation and the model printing accuracy based on the ST dimensions of TB1 and TB2. (A) The measured values for the central ST height and width (in mm) are shown as a function of position within the ST (in degrees from the center of the RW membrane). Segmentation accuracy was evaluated by comparing the dimensions of the cochlea between the scan and the segmentation. For the printing accuracy, the 3D printed SLA and MJ models with the wrapping thickness of 0.3 mm and 0.5 mm were

compared to the segmentation of the cochlea. (B) Comparison of the ST dimensions on the microCT slices of the models to the segmentation of the original cochlea. P-values were calculated with Wilcoxon signed rank test. N = number of measurements.

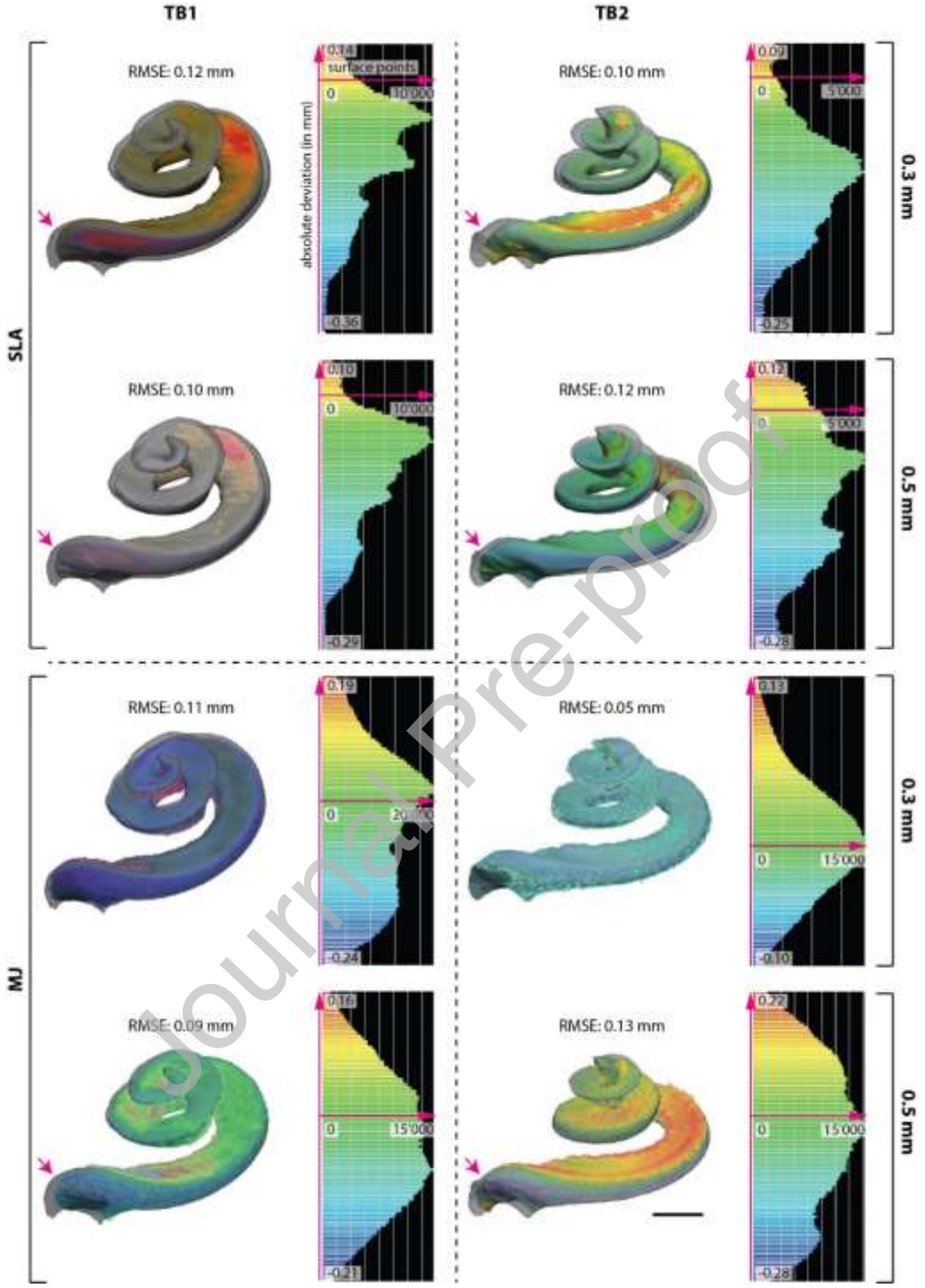

Figure 4. Part comparison analysis between the 3D printed models and the original cochleae of TB1 and TB2. The surfaces of the ST segment of the printed SLA and MJ models (in solid color) with the wrapping thickness of 0.3 mm and 0.5 mm and the original cochleae (in transparent grey) are superimposed. The color-coded histogram next to each model depicts the individual distance/deviation between the closest points of the two surfaces (horizontal axis: number of surface points with a certain deviation; vertical axis: the absolute deviation in mm), which is then represented by a single measurement: the RMSE. Red arrow indicates misalignment due

to a warping deformation of the proximal ST in the 3D printed models. *RMSE: root mean square error* (scale bar: 2 mm)

A Electrode insertion

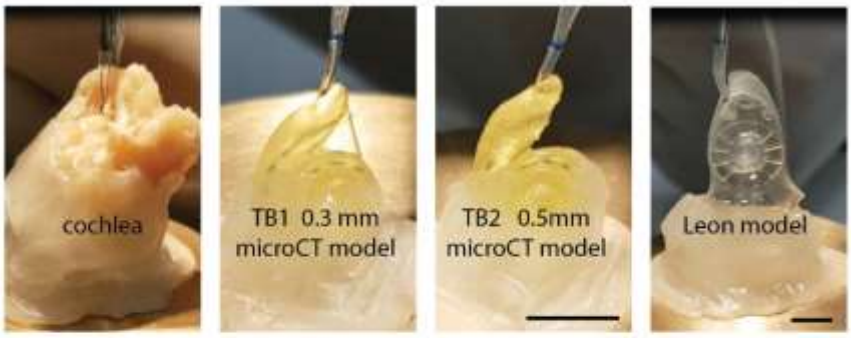

B Insertion and extraction forces as a function of time and insertion depth

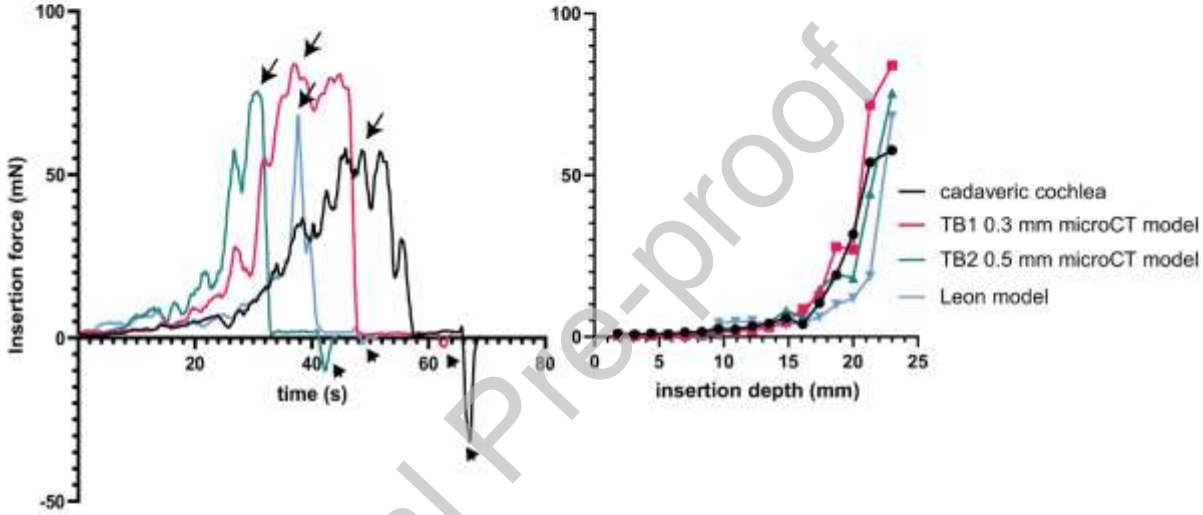

C Comparison of microCT and Leon models to cadaveric cochleae

	cadaveric cochleae (N = 20, 24*)		**microCT models** (N = 24)			**Leon model** (N = 8)		
	mean	sd	mean	sd	p-value	mean	sd	p-value
peak force (mN)#	94.8	64.1	83.2	27.5	0.42	95.3	43.9	0.98
inserted electrodes*	15.4	0.9	15.0	0.9	0.13	15.9	0.4	0.053
overall resistance	0.6	0.6	0.7	0.6	0.52	0.4	0.5	0.45
RW resistance	-0.1	0.9	-0.4	0.6	0.19	-0.1	0.8	0.84
1st turn resistance	0.4	0.6	0.5	0.7	0.45	0.5	0.8	0.62
end resistance	1.5	1.1	1.7	0.9	0.40	0.5	0.8	0.02

D Comparison of anatomically different microCT models

	TB1 microCT model (N = 12)		**TB2 microCT model** (N = 12)		p-value
	mean	sd	mean	sd	
peak force (mN)	96.0	25.4	70.4	24.0	0.006*
inserted electrodes	15.7	0.5	14.3	0.8	<0.0001*
overall resistance	0.6	0.5	0.8	0.6	0.38
RW resistance	-0.4	0.7	-0.3	0.5	0.53
1st turn resistance	0.5	0.7	0.5	0.8	1.00
end resistance	1.3	0.8	2.2	0.7	0.002*

* Significant p ≤ 0.008333 (Bonferroni correction for multiple testing of the six outcome parameters)

Figure 5. Evaluation of mechanical accuracy in comparison to human cadaveric cochleae. (A) Illustration of electrode insertion into real cadaveric cochlea and into the different cochlear models. (scale bars: 5 mm) (B) Positive insertion forces and negative extraction forces as a function of time (on the left) and insertion depth (on the right) for four representative samples with full electrode insertion. Arrows indicate the measured peak forces; arrow points indicate the extraction forces. Only the insertion forces have been analyzed in relation to the insertion depth. (C) Comparison of mechanical characteristics between the models and the cadaveric cochleae. P-value was calculated with non-paired student t test with unequal variances, comparing each model with the real cochleae. N = number of insertions. #Peak forces and number of inserted electrodes were recorded for all insertions (N = 24), whereas tactile feedback in human cadaveric cochleae was only evaluated by CI surgeons (N = 20), who were able to compare it to real-life CI surgery. (D) Comparison of mechanical characteristics between anatomically different microCT models. The insertion peak force, the number of inserted electrodes and the end resistance significantly differed between the anatomically different cochleae. P-value was calculated with linear mixed model analysis, with the operator as the fixed effect. Only SLA models with soap solution were used in this figure and analysis.

3.4. Surgical evaluation

After the experiments, the operators were asked to give a global evaluation of the models. Based on the provided answers, summarized in Table 2, the collective outcome of the operators corresponded to the results of objective mechanical evaluation: (1) SLA models filled with soap corresponded best to the real cochleae, (2) the Leon models and the microCT models were found mechanically equivalent and (3) the wrapping thickness had no effect on the insertion mechanics. The operators showed a preference for microCT models for surgical training and electrode testing due to better correspondence to the real cochlear anatomy. The 0.5 mm models were found to be more robust, especially when printed in SLA, whereas the position of the electrode within the ST could be better estimated in the 0.3 mm models.

	fluid	**3D printing method**	**design**	**thickness**	**morphological preference**	**mechanical preference**	**preference for surgical training**	**preference for electrode testing**
operator 1	soap	=	microCT	=	microCT	=	*	*
operator 2	soap	SLA	=	=	microCT	Leon	microCT	Leon
operator 3	soap	SLA	Leon	=	microCT	=	microCT	microCT
operator 4	soap	=	=	=	microCT	microCT	microCT	microCT
TOTAL	**soap**	**SLA**	**=**	**=**	**microCT**	**=**	**microCT**	**microCT**

Table 2. Summary of the surgical evaluation. *Only experienced CI surgeons (operators 2-4) were asked about their preference for applications, such as surgical training and electrode testing.

4. Discussion

The objective of this study was to develop anatomically and mechanically accurate models of the ST, which are scalable, transparent, robust and representative for surgical electrode insertion through the RW. To achieve this, we designed the models based on the segmentation of the ST and the RW membrane from microCT images of human cadaveric cochleae. The models were produced at the desired scale by using 3D printing technology. The anatomical and mechanical accuracy of the

models were thoroughly evaluated by means of microCT imaging and electrode insertion experiments, performed by experienced cochlear implant surgeons.

For the anatomical evaluation of the models, we distinguished between segmentation and printing accuracy. We found that manual segmentation did not introduce any significant deviations from the original anatomy of the ST, as visualized on the microCT images. The segmentation based on contrast-enhanced microCT imaging (Kerckhofs et al., 2018) in TB2 was easier and slightly more accurate than in TB1, which was imaged using standard microCT after removal of the intracochlear fluid, due to better visualization of the soft-tissue boundaries of the ST. Furthermore, contrast-enhanced microCT with Hf-WD POM enabled us to visualize the cochlear microstructures in a fresh-frozen human sample in a fully nondestructive manner, whereas removal of the intracochlear fluid (Avci et al., 2014; Postnov et al., 2006) and previously used contrast-enhancing staining agents (De Greef et al., 2015; Glueckert et al., 2018; Mukherjee et al., 2012; Rohani et al., 2016; van den Boogert et al., 2018) are destructive, in particular for the soft tissues. Nondestructive 3D visualization of the soft and mineralized intracochlear structures has a promising potential to enable fabrication of more representative cochlear models.

Evaluation of the printing accuracy revealed that 3D printed models showed a good correspondence to the original cochleae. In terms of ST dimensions, the MJ models were more accurate than the SLA models, which were slightly undersized. However, even the average offset of the SLA models (0.11 mm) was well below the inter-individual variability of ST dimensions, which can amount up to 20% or approximately 0.2 mm (Avci et al., 2014; Rebscher et al., 1996). The SLA models were also more prone to general deformations, such as the shift of the proximal ST segment, which mostly occurred during the curing stage, when the SLA model hardens and stress gradients form. This is a known limitation of the SLA additive printing method for very thin objects known as warping (Formlabs, n.d.). More robust design of the external support structure and stabilization of the proximal ST segment in the 0.3 mm wrapping thickness models largely tackled these limitations in our preliminary study, but additional modifications (e.g. slightly oversized printing, more external support structure, low shrinkage resin) may further improve the results in the future. The main limitation of the MJ models was that mechano-chemical removal of the internal support material was also erosive for the models themselves and resulted in a less smooth inner ST surface, compared to the SLA models. In the future, this limitation can be tackled, by using a new-generation soluble support materials for MJ 3D printing, which can be easily removed with non-caustic solutions (Stratasys, n.d.). To the best of our knowledge, this was also the first study, which directly compared the anatomy of the produced models to their original design. This quality-control was crucial for the initial finetuning of 3D printing technology and for the interpretation of mechanical assessment of the models.

The mechanical accuracy of the models was assessed by comparing them to human cadaveric cochleae in a series of electrode insertion experiments. Between two printing technologies (SLA and MJ) and two models of the cochlear fluid (saline and soap solution), the SLA models with soap were found to be the most representative for insertion into the human cadaveric cochlea. Electrode insertion into the MJ models was less smooth and on average one electrode contact less deep due to the erosion of the inner surface, caused by chemical rinsing of the internal support material. Thus, non-smooth surface of the MJ models in fact had a larger effect on the mechanical properties of the insertion than the slightly undersized dimensions of the ST segment in the SLA models. The use of

soap solution resulted in lower friction forces, which was more representative for the insertion mechanics in a real human cochlea, whereby the inner surface is covered with smooth, slippery epithelium (Kontorinis, Paasche, et al., 2011; Rebscher et al., 1996; Todd et al., 2007).

Previous studies evaluated the models, by comparing insertion forces during an automated electrode insertion to human cadaveric cochleae (Aebischer et al., 2021; Leon et al., 2014). In this study, all insertions were done manually by experienced CI surgeons. This approach allowed us to not only accurately reproduce contemporary CI surgery, but also to obtain a surgical evaluation of the insertion mechanics. The recorded force profiles and the measured peak insertion forces in our study were in line with the previous studies (Aebischer et al., 2021; Leon et al., 2014). However, we found that the number of inserted electrodes, the surgically experienced end resistance and the global surgical evaluation were even more sensitive for detection of differences between the models and the human cochleae, than the measured insertion forces. Furthermore, we noticed a discrepancy between the measured insertion forces and the surgically experienced resistance during the testing of models with saline solution, whereby full electrode insertion was usually not possible. In models with saline solution, all surgeons experienced a very high end resistance and electrode buckling, whereas the measured peak insertion forces were significantly lower than for the full insertions into the models with soap solution. This could indicate that the insertion forces increase in a different direction than recorded by our one-dimensional setup. Alternatively, the surgeon might perceive other important cues, such as seeing the electrode buckling, which led them to interrupt the insertion before the insertion forces started increasing. These findings led us to the conclusion that the insertion force measurements and the surgical evaluation are best used complementary with each other to achieve a more representative evaluation of the insertion mechanics.

The insertion mechanics were also compared between our anatomical microCT models and the RW models of (Leon et al., 2014). According to our evaluation, both models were fully mechanically representative for the group of human cadaveric cochleae. However, anatomical differences within the microCT models had an additional clear influence on the insertion forces, the number of inserted electrodes and the end resistance: in TB2, we recorded higher end resistance and more incomplete insertions. Previous studies reported that insertion into smaller cochleae (smaller cochlear volume, smaller cochlear width) is associated with higher insertion forces (Dhanasingh et al., 2021) and a higher risk of residual hearing loss after CI surgery (Takahashi et al., 2018). In our study, TB2 was in fact larger than TB1, but its ST was narrower, which resulted in the more difficult insertion and also indicates that the internal dimensions of the ST may not always be related to the overall size of the cochlea. The insertion peak forces were also lower in TB2, which may be explained by the surgeon's preference to tolerate a slightly incomplete insertion rather than push the electrode into the ST against high resistance. These results confirm the existing link between cochlear anatomy and electrode insertion mechanics (Avci et al., 2014; Demarcy et al., 2017; Dhanasingh et al., 2021; Takahashi et al., 2018; Verbist et al., 2009), illustrate the potential of our anatomical models to study this relation in a controlled, repeatable way, and warrant further study to disentangle which anatomical features have a direct effect on the insertion mechanics. Another important advantage of our models, compared to the previous designs, is their anatomical outer shape, which makes them more representative for real-life CI surgery. This shape was achieved by creating a semi-uniform wrapping around the ST segment, rather than embedding the hollow ST inside a non-anatomical shape (Aebischer et al., 2021; Clark et al., 2011; Leon et al., 2014; Majdani et al., 2010a; Rebscher et al., 1996; Todd et al., 2007; Zhang et al., 2010). Two wrapping thicknesses were tested: 0.3 mm and

0.5 mm for a 1:1 scale model. As expected, both designs were mechanically equivalent, but the transparency and the visualization of the electrode position was substantially better in the 0.3 mm models. The SLA 0.3 mm models were somewhat more fragile, but with gentle handling, also these models remained intact and functional during repeated insertions.

Our models were developed and tested for electrode insertion studies, whereby our primary objective was to replicate the surgical RW approach. We were able to incorporate the individual anatomical shape, dimensions and position of the RW in our model design. Insertion through the RW is considered to be less traumatic, if it is feasible and can be performed without complications (Roland et al., 2007; Schart-Morén et al., 2019). Furthermore, the RW is an interesting access point for the administration of next-generation inner ear therapies into the cochlea (Devare et al., 2018). However, in some cases, the proximal ST can be significantly narrowed by an extrusion in the outer wall – called the crista fenestra – which can lead to electrode deviation and trauma in RW insertion (Angeli et al., 2017; Atturo et al., 2014). Insertion experiments in anatomical models of human cochleae can help us understand the insertion mechanics and develop better strategies to avoid trauma. For example, studies in cochlear models can help us determine whether atraumatic insertion through the RW would be feasible or a cochleostomy approach would be preferable instead. Whereas our models were mainly developed for insertion through the RW, their anatomical design and realistic outer shape enables the surgeon to also drill a cochleostomy in its usual position, just below the RW. In addition to development and testing of novel surgical techniques and CI electrode designs, our models can be used for training of CI surgeons. To achieve optimal simulation of the intraoperative environment, the ST models can be incorporated in artificial temporal bones (Roosli et al., 2013) and used for drilling practice. Furthermore, CT-based modelling of patient anatomy can be used for pre-operative planning of CI surgery.

Our study did have some limitations. All standardized insertion experiments were conducted with one electrode type, Advanced Bionics HiFocus™ SlimJ straight electrode. The feasibility of full insertion into the produced models was only briefly tested for two other electrodes: a Cochlear Nucleus® slim modiolar electrode CI632 and a slim straight electrode 522 (Cochlear Ltd., Sydney, Australia). A straight electrode by design follows the outer wall of the ST, which results in higher friction forces, than with a perimodiolar insertion (Todd et al., 2007; Zhang et al., 2009). This likely resulted in larger differences between models with different characteristics (printing technology, fluid model), than if a perimodiolar electrode would have been used and also facilitated the detection of differences models and the human cadaveric cochleae. In addition, while the analysis of outcome parameters did not show any significant differences in the insertion mechanics between the SLA models with soap and the cadaveric cochleae, two surgeons nevertheless found the insertion into the models less smooth. Future application of specialized coating onto the internal surface of the model could potentially further optimize the insertion mechanics in the cochlear models (Aebischer et al., 2021). Finally, whereas manual electrode insertions enabled evaluation of the surgical tactile feedback, they are by design less repeatable and controllable (e.g. constant insertion speed, insertion vector) than automated insertions (Breinbauer & Praetorius, 2015; Kontorinis, Lenarz, et al., 2011). In the future experiments, both approaches can be combined to obtain an in-depth understanding of the interplay between cochlear anatomy and electrode insertion mechanics.

5. Conclusion

To summarize, this paper describes in detail how to produce and test ST models, which are anatomically, surgically and mechanically representative for electrode insertion through the RW in human cadaveric cochleae. These models can be used to investigate the interplay between the individual cochlear anatomy and the insertion mechanics of cochlear implants and other inner ear therapies in a controlled, repeatable way. Better understanding of the relation between the anatomy and the insertion mechanics, influenced by surgical techniques and electrode design, will help prevent cochlear insertion trauma. The proposed model design not only opens many new possibilities for preclinical testing of next-generation surgical techniques and electrode designs, but will also enable realistic surgical training and preoperative planning for patient-tailored CI surgery.

Acknowledgements

This work was supported by Flemish Research Foundation (FWO/ 1804816N, 12Y6919N, 1S78519N, 1S78521N) and by the Internal Funds of the KU Leuven. We thank the colleagues of the Vesalius Institute, KU Leuven and the Mortuary of the UZ Leuven for their help in harvesting and preserving the temporal bones, as well as the anonymous donors of the temporal bones. We thank the KU Leuven XCT core facility for providing access to the XCT infrastructure to record microCT data. We thank Carla Geeroms for her help with the acquisition of microCT data, and Tim Balcaen together with Prof. Dr. Wim De Borggraeve for their help with the synthesis of the Hafnium-substituted Wells-Dawson polyoxometalate. We thank Advanced Bionics and Cochlear Limited for providing electrode arrays, used in this study. We thank Dr. Gideon Wackers for his help with chemical rinsing of the models. We thank Prof. Emmanuel Mylanus and Prof. Christian Desloovere for their help with mechanical evaluation of the models. We thank Tine Arras and Prof. Dr. Geert Molenberghs for their advice and help with statistical analysis of the data.

Author contributions

A.S., E.S., T.P. and N.V. designed research; A.S., E.S., T.P. and N.V. performed research. A.S., E.S., T.P., G.K., J.W. and N.V. analyzed data; A.S. wrote the original draft; A.S., E.S., T.P., G.K., C.P., J.W. and N.V. reviewed and edited the manuscript.

Competing interest statement

The authors declare no conflict of interest.

Author Statement for the manuscript, titled:

A.S., E.S., T.P. and N.V. designed research; A.S., E.S., T.P. and N.V. performed research. A.S., E.S., T.P., G.K., J.W. and N.V. analyzed data; A.S. wrote the original draft; A.S., E.S., T.P., G.K., C.P., J.W. and N.V. reviewed and edited the manuscript.

References

Advanced Bionics. (n.d.). *Surgeon's Manual for the HiRes ™ Ultra 3D Cochlear Implant with the HiFocus ™ SlimJ and HiFocus ™ Mid-Scala Electrodes*. Advanced Bionics. Retrieved June 27, 2022, from https://www.advancedbionics.com/content/dam/advancedbionics/Documents/Regional/US/Professional

s/HiRes-Ultra 3D-Surgeons-Manual-FDA.pdf

Aebischer, P., Caversaccio, M., & Wimmer, W. (2021). Fabrication of human anatomy-based scala tympani models with a hydrophilic coating for cochlear implant insertion experiments. *Hearing Research*, *404*, 108205. https://doi.org/10.1016/J.HEARES.2021.108205

Aebischer, P., Mantokoudis, G., Weder, S., Anschuetz, L., Caversaccio, M., & Wimmer, W. (2022). In-Vitro Study of Speed and Alignment Angle in Cochlear Implant Electrode Array Insertions. *IEEE Transactions on Biomedical Engineering*, *69*(1), 129–137. https://doi.org/10.1109/TBME.2021.3088232

Angeli, R. D., Lavinsky, J., Setogutti, E. T., & Lavinsky, L. (2017). The Crista Fenestra and Its Impact on the Surgical Approach to the Scala Tympani during Cochlear Implantation. *Audiology & Neuro-Otology*, *22*(1), 50–55. https://doi.org/10.1159/000471840

Atturo, F., Barbara, M., & Rask-Andersen, H. (2014). On the Anatomy of the "Hook" Region of the Human Cochlea and How It Relates to Cochlear Implantation. *Audiol Neurotol*, *19*, 378–385. https://doi.org/10.1159/000365585

Avci, E., Nauwelaers, T., Lenarz, T., Hamacher, V., & Kral, A. (2014). Variations in microanatomy of the human cochlea. *The Journal of Comparative Neurology*, *522*(14), 3245–3261. https://doi.org/10.1002/cne.23594

Bas, E., Dinh, C. T., Garnham, C., Polak, M., & Van de Water, T. R. (2012). Conservation of hearing and protection of hair cells in cochlear implant patients' with residual hearing. *Anatomical Record*, *295*(11), 1909–1927. https://doi.org/10.1002/ar.22574

Breinbauer, H. A., & Praetorius, M. (2015). Variability of an ideal insertion vector for cochlear implantation. *Otology and Neurotology*, *36*(4), 610–617. https://doi.org/10.1097/MAO.0000000000000719

Briggs, R. J. S., Tykocinski, M., Lazsig, R., Aschendorff, A., Lenarz, T., Stöver, T., Fraysse, B., Marx, M., Thomas Roland, J., Roland, P. S., Wright, C. G., Gantz, B. J., Patrick, J. F., & Risi, F. (2011). Development and evaluation of the modiolar research array - multi-centre collaborative study in human temporal bones. *Cochlear Implants International*, *12*(3), 129–139. https://doi.org/10.1179/1754762811Y0000000007

Clark, J. R., Warren, F. M., & Abbott, J. J. (2011). A Scalable Model for Human Scala-Tympani Phantoms. *Journal of Medical Devices*, *5*(1), 014501. https://doi.org/10.1115/1.4002932

Conde-Valverde, M., Martínez, I., Quam, R. M., Bonmatí, A., Lorenzo, C., Velez, A. D., Martínez-Calvo, C., & Arsuaga, J. L. (2019). The cochlea of the Sima de los Huesos hominins (Sierra de Atapuerca, Spain): New insights into cochlear evolution in the genus Homo. *Journal of Human Evolution*, *136*, 102641. https://doi.org/10.1016/j.jhevol.2019.102641

De Greef, D., Buytaert, J. A. N., Aerts, J. R. M., Van Hoorebeke, L., Dierick, M., & Dirckx, J. (2015). Details of human middle ear morphology based on micro-CT imaging of phosphotungstic acid stained samples. *Journal of Morphology*, *276*(9), 1025–1046. https://doi.org/10.1002/jmor.20392

De Seta, D., Daoudi, H., Torres, R., Ferrary, E., Sterkers, O., & Nguyen, Y. (2022). Robotics, automation, active electrode arrays, and new devices for cochlear implantation: A contemporary review. *Hearing Research*, *414*, 108425. https://doi.org/10.1016/J.HEARES.2021.108425

Demarcy, T., Vandersteen, C., Guevara, N., Raffaelli, C., Gnansia, D., Ayache, N., & Delingette, H. (2017). Automated analysis of human cochlea shape variability from segmented µCT images. *Computerized Medical Imaging and Graphics*, *59*, 1–12. https://doi.org/10.1016/j.compmedimag.2017.04.002

Devare, J., Gubbels, S., & Raphael, Y. (2018). Outlook and future of inner ear therapy. In *Hearing Research* (Vol. 368, pp. 127–135). Elsevier. https://doi.org/10.1016/j.heares.2018.05.009

Dhanasingh, A., Swords, C., Bance, M., Van Rompaey, V., & Van de Heyning, P. (2021). Cochlear Size Assessment Predicts Scala Tympani Volume and Electrode Insertion Force- Implications in Robotic Assisted Cochlear Implant Surgery. *Frontiers in Surgery*, *8*, 723897. https://doi.org/10.3389/FSURG.2021.723897

Erixon, E., Högstorp, H., Wadin, K., & Rask-Andersen, H. (2009). Variational Anatomy of the Human Cochlea. *Otology & Neurotology*, *30*(1), 14–22. https://doi.org/10.1097/MAO.0b013e31818a08e8

Formlabs. (n.d.). *Best practices for post-curing prints*. Formlabs. Retrieved November 24, 2022, from https://support.formlabs.com/s/article/Best-practices-for-post-curing-prints?language=en_US

Glueckert, R., Johnson Chacko, L., Schmidbauer, D., Potrusil, T., Pechriggl, E. J., Hoermann, R., Brenner, E., Reka, A., Schrott-Fischer, A., & Handschuh, S. (2018). Visualization of the Membranous Labyrinth and Nerve Fiber Pathways in Human and Animal Inner Ears Using MicroCT Imaging. *Frontiers in Neuroscience*, *12*, 501. https://doi.org/10.3389/fnins.2018.00501

Hoskison, E., Mitchell, S., & Coulson, C. (2017). Systematic review: Radiological and histological evidence of cochlear implant insertion trauma in adult patients. *Cochlear Implants International*, *18*(4), 192–197. https://doi.org/10.1080/14670100.2017.1330735

Kendi, T. K., Arikan, O. K., & Koc, C. (2005). Volume of components of labyrinth: Magnetic resonance imaging

study. *Otology and Neurotology*, *26*(4), 778–781. https://doi.org/10.1097/01.mao.0000169635.25322.9e

Kerckhofs, G., Stegen, S., van Gastel, N., Sap, A., Falgayrac, G., Penel, G., Durand, M., Luyten, F. P., Geris, L., Vandamme, K., Parac-Vogt, T., & Carmeliet, G. (2018). Simultaneous three-dimensional visualization of mineralized and soft skeletal tissues by a novel microCT contrast agent with polyoxometalate structure. *Biomaterials*, *159*, 1–12. https://doi.org/10.1016/j.biomaterials.2017.12.016

Kirk, E. C., & Gosselin-Ildari, A. D. (2009). Cochlear Labyrinth Volume and Hearing Abilities in Primates. *The Anatomical Record: Advances in Integrative Anatomy and Evolutionary Biology*, *292*(6), 765–776. https://doi.org/10.1002/ar.20907

Kontorinis, G., Lenarz, T., Stöver, T., & Paasche, G. (2011). Impact of the insertion speed of cochlear implant electrodes on the insertion forces. *Otology and Neurotology*, *32*(4), 565–570. https://doi.org/10.1097/MAO.0b013e318219f6ac

Kontorinis, G., Paasche, G., Lenarz, T., & Stöver, T. (2011). The effect of different lubricants on cochlear implant electrode insertion forces. *Otology and Neurotology*, *32*(7), 1050–1056. https://doi.org/10.1097/MAO.0b013e31821b3c88

Lenarz, T. (2017). Cochlear implant - state of the art. *GMS Current Topics in Otorhinolaryngology, Head and Neck Surgery*, *16*, Doc04. https://doi.org/10.3205/cto000143

Leon, L., Cavilla, M. S., Doran, M. B., Warren, F. M., & Abbott, J. J. (2014). Scala-Tympani Phantom With Cochleostomy and Round-Window Openings for Cochlear-Implant Insertion Experiments. *Journal of Medical Devices*, *8*(4), 041010. https://doi.org/10.1115/1.4027617

Maes, A., Pestiaux, C., Marino, A., Balcaen, T., Leyssens, L., Vangrunderbeeck, S., Pyka, G., De Borggraeve, W. M., Bertrand, L., Beauloye, C., Horman, S., Wevers, M., & Kerckhofs, G. (2022). Cryogenic contrast-enhanced microCT enables nondestructive 3D quantitative histopathology of soft biological tissues. *Nature Communications*, *13*(1), 6207. https://doi.org/10.1038/s41467-022-34048-4

Majdani, O., Schurzig, D., Hussong, A., Rau, T., Wittkopf, J., Lenarz, T., & Labadie, R. F. (2010a). Force measurement of insertion of cochlear implant electrode arrays in vitro: Comparison of surgeon to automated insertion tool. *Acta Oto-Laryngologica*, *130*(1), 31–36. https://doi.org/10.3109/00016480902998281

Majdani, O., Schurzig, D., Hussong, A., Rau, T., Wittkopf, J., Lenarz, T., & Labadie, R. F. (2010b). *Force measurement of insertion of cochlear implant electrode arrays in vitro: comparison of surgeon to automated insertion tool*. *130*(1), 31–36. https://doi.org/10.3109/00016480902998281

Mukherjee, P., Uzun-Coruhlu, H., Wong, C. C., Curthoys, I. S., Jones, A. S., & Gibson, W. P. R. (2012). Assessment of intracochlear trauma caused by the insertion of a new straight research array. *Cochlear Implants International*, *13*(3), 156–162. https://doi.org/10.1179/1754762811Y.0000000013

Postnov, A., Zarowski, A., De Clerck, N., Vanpoucke, F., Offeciers, F. E., Van Dyck, D., & Peeters, S. (2006). High resolution micro-CT scanning as an innovatory tool for evaluation of the surgical positioning of cochlear implant electrodes. *Acta Oto-Laryngologica*, *126*(5), 467–474. https://doi.org/10.1080/00016480500437377

Rebscher, S. J., Talbot, N., Bruszewski, W., Heilmann, M., Brasell, J., & Merzenich, M. M. (1996). A transparent model of the human scala tympani cavity. *Journal of Neuroscience Methods*, *64*(1), 105–114. https://doi.org/10.1016/0165-0270(95)00116-6

Rohani, S. A., Ghomashchi, S., Umoh, J., Holdsworth, D. W., Agrawal, S. K., & Ladak, H. M. (2016). Iodine potassium iodide improves the contrast-to-noise ratio of micro-computed tomography images of the human middle ear. *Journal of Microscopy*, *264*(3), 334–338. https://doi.org/10.1111/JMI.12447/FORMAT/PDF

Roland, P. S., Wright, C. G., & Isaacson, B. (2007). Cochlear Implant Electrode Insertion: The Round Window Revisited. *The Laryngoscope*, *117*(8), 1397–1402. https://doi.org/10.1097/MLG.0b013e318064e891

Roosli, C., Sim, J. H., Möckel, H., Mokosch, M., & Probst, R. (2013). An artificial temporal bone as a training tool for cochlear implantation. *Otology and Neurotology*, *34*(6), 1048–1051. https://doi.org/10.1097/MAO.0b013e31828f4907

Schart-Morén, N., Agrawal, S. K., Ladak, H. M., Li, H., & Rask-Andersen, H. (2019). Effects of Various Trajectories on Tissue Preservation in Cochlear Implant Surgery: A Micro-Computed Tomography and Synchrotron Radiation Phase-Contrast Imaging Study. *Ear & Hearing*, *40*(2), 393–400. https://doi.org/10.1097/AUD.0000000000000624

Shin, K.-J., Lee, J.-Y., Kim, J.-N., Yoo, J.-Y., Shin, C., Song, W.-C., & Koh, K.-S. (2013). Quantitative Analysis of the Cochlea using Three-Dimensional Reconstruction based on Microcomputed Tomographic Images. *The Anatomical Record*, *296*(7), 1083–1088. https://doi.org/10.1002/ar.22714

Snels, C., Roland, J. T., Treaba, C., Jethanamest, D., Huinck, W., Friedmann, D. R., Dhooge, I., & Mylanus, E.

(2021). Force and pressure measurements in temporal bones. *American Journal of Otolaryngology*, *42*(2), 102859. https://doi.org/10.1016/j.amjoto.2020.102859

Starovoyt, A., Putzeys, T., Wouters, J., & Verhaert, N. (2019). High-resolution Imaging of the Human Cochlea through the Round Window by means of Optical Coherence Tomography. *Scientific Reports*, *9*(1), 14271. https://doi.org/10.1038/s41598-019-50727-7

Stratasys. (n.d.). *3D Printer Materials for Polyjet 3D Printing*. Retrieved June 14, 2022, from https://www.stratasys.com/en/materials/materials-catalog/?filter=MT_PolyJet

Takahashi, M., Arai, Y., Sakuma, N., Yabuki, K., Sano, D., Nishimura, G., Oridate, N., & Usami, S. ichi. (2018). Cochlear volume as a predictive factor for residual-hearing preservation after conventional cochlear implantation. *Acta Oto-Laryngologica*, *138*(4), 345–350. https://doi.org/10.1080/00016489.2017.1393840

Tinne, N., Antonopoulos, G. C., Mohebbi, S., Andrade, J., Nolte, L., Meyer, H., Heisterkamp, A., Majdani, O., & Ripken, T. (2017). Three-dimensional hard and soft tissue imaging of the human cochlea by scanning laser optical tomography (SLOT). *PLOS ONE*, *12*(9), e0184069. https://doi.org/10.1371/journal.pone.0184069

Todd, C. A., Naghdy, F., & Svehla, M. J. (2007). Force application during cochlear implant insertion: An analysis for improvement of surgeon technique. *IEEE Transactions on Biomedical Engineering*, *54*(7), 1247–1255. https://doi.org/10.1109/TBME.2007.891937

van den Boogert, T., van Hoof, M., Handschuh, S., Glueckert, R., Guinand, N., Guyot, J.-P., Kingma, H., Perez-Fornos, A., Seppen, B., Johnson Chacko, L., Schrott-Fischer, A., & van de Berg, R. (2018). Optimization of 3D-Visualization of Micro-Anatomical Structures of the Human Inner Ear in Osmium Tetroxide Contrast Enhanced Micro-CT Scans. *Frontiers in Neuroanatomy*, *12*, 41. https://doi.org/10.3389/fnana.2018.00041

van der Marel, K. S., Briaire, J. J., Wolterbeek, R., Snel-Bongers, J., Verbist, B. M., & Frijns, J. H. M. (2014). Diversity in Cochlear Morphology and Its Influence on Cochlear Implant Electrode Position. *Ear & Hearing*, *35*(1), e9–e20. https://doi.org/10.1097/01.aud.0000436256.06395.63

Verbist, B. M., Ferrarini, L., Briaire, J. J., Zarowski, A., Admiraal-Behloul, F., Olofsen, H., Reiber, J. H. C., & Frijns, J. H. M. (2009). Anatomic considerations of cochlear morphology and its implications for insertion trauma in cochlear implant surgery. *Otology and Neurotology*, *30*(4), 471–477. https://doi.org/10.1097/MAO.0b013e3181a32c0d

Verbist, B. M., Skinner, M. W., Cohen, L. T., Leake, P. A., James, C., Boëx, C., Holden, T. A., Finley, C. C., Roland, P. S., Roland, J. T., Haller, M., Patrick, J. F., Jolly, C. N., Faltys, M. A., Briaire, J. J., & Frijns, J. H. M. (2010). Consensus Panel on a Cochlear Coordinate System Applicable in Histologic, Physiologic, and Radiologic Studies of the Human Cochlea. *Otology & Neurotology*, *31*(5), 722–730. https://doi.org/10.1097/MAO.0b013e3181d279e0

Zhang, J., Roland, J. T., Manolidis, S., & Simaan, N. (2009). Optimal path planning for robotic insertion of steerable electrode arrays in cochlear implant surgery. *Journal of Medical Devices, Transactions of the ASME*, *3*(1), 1–10. https://doi.org/10.1115/1.3039513

Zhang, J., Wei, W., Ding, J., Roland, J. T., Manolidis, S., & Simaan, N. (2010). Inroads Toward Robot-Assisted Cochlear Implant Surgery Using Steerable Electrode Arrays. *Otology & Neurotology*, *31*(8), 1199–1206. https://doi.org/10.1097/MAO.0b013e3181e7117e